J Mater Sci (2008) 43:2171–2178
DOI 10.1007/s10853-007-2032-9

Hydrothermal synthesis of hydroxyapatite whiskers with sharp faceted hexagonal morphology

Inés S. Neira · Francisco Guitián · Takaaki Taniguchi · Tomoaki Watanabe · Masahiro Yoshimura

Received: 28 October 2006 / Accepted: 20 July 2007 / Published online: 22 December 2007

Abstract We report an effective method for the synthesis of hydroxyapatite whiskers with sharp faceted hexagonal shape employing a low temperature (90 °C) hydrothermal route with calcium nitrate tetrahydrate, diammonium phosphate and urea as starting materials. The key parameters of the synthesis process i.e. duration, temperature cycle of the treatment and starting pH value are carefully varied and the end products are investigated using powder X-ray diffraction (XRD), Raman-scattering, infrared spectroscopy (IR), elemental analysis, scanning electron microscopy (SEM), energy-dispersive X-ray spectroscopy (EDX), transmission electron microscopy (TEM), electron diffraction (ED), and high-resolution TEM (HRTEM) in order to find the optimal reaction conditions that lead to the desired hexagonal morphology of HA whiskers. The results demonstrate that gradual and greater increase in solution pH during the hydrothermal process favors large quantity of the single-crystalline hydroxyapatite whiskers with well defined hexagonal morphology.

Introduction

Hydroxyapatite ($Ca_{10}(PO_4)_6(OH)_2$, identified as HA from now onwards) ceramics are excellently biocompatible and osteoconductive (they enhance bone formation by acting as a scaffold on which bone cells can attach and grow) [1]. They are widely studied as an alternative to natural bone grafts because they do not present limitations in availability, potential disease transmission and/or risk of rejection which commonly occurs in natural bone materials. However the fracture toughness parameter of HA is lower than that reported for natural human bones (~1 MPa/m^2 in front of 2–12 MPa/m^2) [2], and thus, till now, its applications are limited to areas where bones are free of dynamic load i.e. for non-load bearing, for craniofacial and periodontal applications, for coatings [3, 4], or as materials for the development of scaffolds for bone tissue engineering [5, 6]. One of the most studied methods to improve the mechanical properties of HA ceramics is the addition of whiskers. Since it is well known that various fibrous bioinert materials that have been applied in HA ceramics such as SiC, C, Si_3N_4, Al_2O_3 or ZrO_2 decrease the biocompatibility and bioactivity of this ceramics [7–9], the investigation of HA with rod-like morphology have recently received much attention [10]. They have been synthesized by various methods, mainly by hydrothermal synthesis [11–13] or homogenous precipitation [14–16], and to a lesser extent, by growth in the gel system [17], molten salts synthesis [18], electrochemical deposition [19] and liquid–solid–solution synthesis [20]. Products prepared by molten salts reaction and in the gel system show important dependence on the preparation conditions. Moreover, with the molten salts method, the obtained crystals incorporates K^+ ions, and therefore, they could not be regarded as pure HA whiskers. Under hydrothermal conditions and homogeneous precipitation, crystalline HA particles can be successfully synthesized, but the particles mostly posses needle-like shape [21–25].

I. S. Neira · T. Taniguchi · T. Watanabe · M. Yoshimura (✉)
Materials and Structures Laboratory, Tokyo Institute of Technology, 4259 Nagatsuta, Midori-ku, Yokohama 226-8503, Japan
e-mail: yoshimura@msl.titech.ac.jp

I. S. Neira · F. Guitián
Instituto de Cerámica de Galicia, Universidade de Santiago de Compostela, Santiago de Compostela 15782, Spain

Although a numerous mentioned above approaches that have been already realized for the fabrication of HA with rod-like morphology (nanorods, needles, wires, fibres, etc.), some problems are still unsettled, namely, there are just few reports of preparation of HA whiskers with hexagonal morphology in literature [18, 26, 27]. Moreover, these synthetic procedures are not well developed in terms of phase purity, homogeneity of microstructural characteristics (well-defined hexagonal whisker shape, narrower particle size range, etc.), and feasibility of large-scale production, as it is reasonably expected to be in a slower, moderate-temperature hydrothermal context.

In this work, we present the hydrothermal route to HA whiskers with sharp faceted hexagonal prism morphology. This approach to HA whiskers may be useful for the detailed experimental investigation on shape-dependent mechanical properties of HA ceramics.

Experimental

Materials

$Ca(NO_3)_2 \cdot 4H_2O$ (98.5%, Wako), $(NH_4)_2HPO_4$ (99.0%, Wako), $(NH_2)_2CO$ (urea, 99.0%, Wako), HNO_3 (63%, Wako) and $C_{16}H_{33}N(CH_3)_3Br$ (Cetyltrimethylammonium bromide (CTAB), 98%, Wako) were used as received. Distilled water was also used during the hydrothermal process as well as for the preparation of the aqueous solution of nitric acid.

Hydrothermal syntheses

$Ca(NO_3)_2 \cdot 4H_2O$ (5.84 mmol), $(NH_4)_2HPO_4$ (3.50 mmol) (Ca/P molar ratio: 1.67) and urea (17.5 mmol) were mixed with 25 mL of distilled water in a polytretrafluoroethylene (PTFE) vessel (volume-40 mL). The pH was then adjusted to the 3–3.5 range by diluted 0.5 M $HNO_{3(aq)}$ using a Mettler Toledo InLab 413SG pH-meter. The vessel was capped by a PTFE cover and placed inside a stainless steel autoclave. A 1.5 mm thick, low density (0.6 g/cm^3) HYPER-SHEET gasket (GORE-TEX) with porous structure of PTEF polymer was placed between the vessel and the cover, which enables gradual release of the CO_2 forming during the urea decomposition under hydrothermal conditions. The sealed autoclave was subject to treatments of different temperature cycles (Table 1; Fig. 1) as well as several additional syntheses were performed at lower temperatures and durations. One additional synthesis was performed together with CTAB as a surfactant under critical micelle point (9.2×10^{-4} mol/L).

The product of the hydrothermal process was collected by filtration, washed four times with distilled water and once with ethanol, and then dried at 80 °C for 12 h on air. Throughout this work, a set of acronyms is used (Table 1) where the Roman characters mean the number of the sample follows.

Characterization

The products were characterized by powder X-ray diffraction (XRD) using a Rigaku RINT 2000 diffractometer with Ni-filtered CuK_α radiation (λ = 1.54178 Å), operating at 200 mA and 50 kV. Data were collected in the 2θ range of 3–70°, with a scan speed of 1°/min, and a step width of 0.02°.

The room temperature Raman scattering measurements were carried out on a Jobin Yvon T64000 spectrometer with visible Ar^+ laser light (λ = 514.532 nm) as the excitation light. The slits were adjusted so that the resolution was 1 cm^{-1}. All measurements were carried out under the microscope (the laser spot diameter was estimated to be between 1 μm and 2 μm).

The room temperature diffuse reflectance infrared (IR) Fourier-transform spectra were recorded on a Jeol JIR-7000 spectrometer with a resolution of 4 cm^{-1} and a scan time of 10. The crystalline products (~4 mg) were thoroughly grinded with (~200 mg) potassium bromide powder (KBr for IR, Wako) in an agate mortar and pestle to give a fine mixture, and subjected to IR analysis. For the background spectrum, a fine grinded KBr powder was used.

Carbon content was quantitatively determined by combustion bulk elemental analysis using a Fisons EA 1108 elemental analyzer.

The morphology and structure were studied by scanning electron microscopy (SEM) using a Hitachi S-4500 microscope operating at 15 kV, transmission electron microscopy (TEM), electron diffraction (ED) and high-resolution TEM (HRTEM) using a Hitachi H-8100 microscope operating at 200 kV. The samples for transmission electron microscopy were dispersed in ethanol and deposited on a holey carbon grid.

Energy-dispersive X-ray spectroscopy (EDX) for semi-quantitative Ca and P content determination was performed with a EDAX DX-95 spectrometer using commercial hydroxyapatite powder (HW-003, Mitsubishi Chemicals) as a standard sample (molar ratio Ca/P = 1.67).

Results

Hydrothermal synthesis

HA whiskers were prepared by a reaction between $Ca(NO_3)_2 \cdot 4H_2O$ and $(NH_4)_2HPO_4$ (Ca/P molar

Table 1 Summary of the selected hydrothermal reactions

Sample	Synthesis condition	pH_{final}	Phase composition	
			XRD	Raman
I	90 °C, 72 h	8.4	HA	HA
II	Scheme 1	8.6	HA	HA
III	Scheme 2	6.9	OCP[b] + HA + DCPA[c]	OCP[b] + HA + DCPA[c]
IV[a]	Scheme 2	7.5	OCP[b] + HA	OCP[b] + HA

[a] CTAB is used as a surfactant

[b] Major amount of the octacalcium phosphate phase ($Ca_8H_2(PO_4)_6 \cdot 5H_2O$, OCP)

[c] Minor amount of the dicalcium phosphate anhydrous phase ($CaHPO_4$, DCPA)

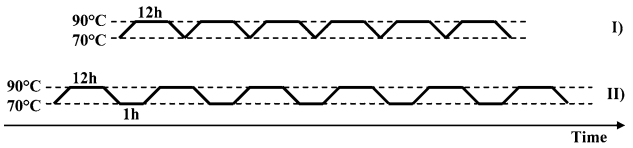

Fig. 1 Schemes of the temperature cycles applied during the experimental procedure. The temperature increasing and decreasing step was 0.5 °C/min in case of Scheme 1 and 1 h ramping at 70 °C in Scheme 2

ratio = 1.67) under hydrothermal conditions. The precursors were chosen to avoid contamination of the precipitate by incorporation of others foreign ions like K^+, Na^+, etc. Urea was utilized as a homogenous precipitation agent, since its decomposition (85–95 °C) releases $NH_{3(aq)}$ to the reaction medium which in turn gradually increase the pH.

The summary from selected hydrothermal syntheses is given in Table 1. Analysis of the obtained data reveals that important parameters for the hydrothermal synthesis of the title compound are temperature, duration, and the initial pH. The optimal values were found to be $T = 90$ °C, $t = 72$ h, and starting pH = 3.0–3.5. All our attempts to reduce the temperature and/or duration of the hydrothermal treatment as well as other starting pH range do not lead to the phase pure HA.

In order to improve the quantity of HA whiskers with well-defined hexagonal prism shape, two different temperature cycles of treatment were applied with the aim of gradually increasing the pH during the synthesis by decreasing the temperature under the urea decomposition point to interrupt it, and thus hold up the NH_3 release (Fig. 1; Table 1). It was observed that Scheme 1 (Fig. 1) results in the highest quantity of the pure HA phase whiskers with sharp faceted hexagonal shape, while all the syntheses following Scheme 2 (Fig. 1) drastically reduced the yield, although the application of a surfactant (CTAB) during the same provides possibility to obtain HA whiskers with relatively uniform size distribution (*vide infra*).

Powder X-Ray diffraction

The powder XRD pattern of the samples reveals the overall crystalline structure of the products (Fig. 2). According to the phase analysis, the patterns of the samples **I** and **II** are nearly the same and also confirm the formation of a pure phase hydroxyapatite by comparison with standard database (JCPDS No. 72-1243). However, there are some inconsistencies between the intensity of the XRD reflections corresponding to the (100), (200) and (300) diffraction peaks reported in JCPDS database and the observed ones (inset in Fig. 2); it is caused by the texturing of whisker particles samples. These results demonstrate that the as-produced HA is mainly oriented along the *c*-axis direction of the hexagonal crystal structure [18, 28].

A different result is obtained in case of samples **III** and **IV**. According to the XRD analysis (Fig. 2; Table 1) sample **III** consists of octacalcium phosphate (OCP) (JCPDS No. 74-1301), hydroxyapatite (JCPDS No. 72-1243) and dicalcium phosphate anhydrous (DCPA) (JCPDS No. 70-1425) where OCP is the main phase along with 30 wt.% of HA and a minor amount of the DCPA by-product. OCP and HA has similar structures and a rough estimation of wt.% content was made from comparison of the intensities of the main diffraction peaks after background correction, since the Rietveld profile refinement was not possible on this complex mixture. Generally powder XRD of sample **IV** is similar to that from **III** (Fig. 2), but this powder has less DCPA by-product (~10 times) and less HA (~3 times).

Raman scattering

Figure 3 shows the Raman spectra collected from the samples. The set of observed Raman bands agrees fairly well with the phase composition reported by XRD technique, which reveals that samples **I** and **II** contains pure HA only, while samples **III** and **IV** are mixtures of OCP as the most abundant phase and HA.

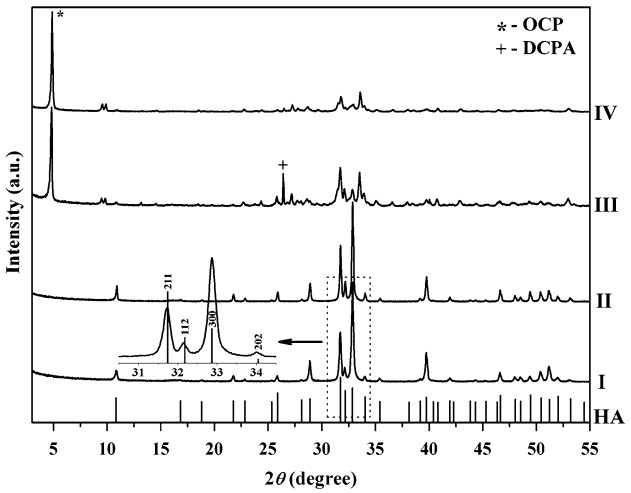

Fig. 2 Comparison of the powder diffraction patterns for the samples **I**, **II**, **III** and **IV**. An inset shows the enlarged region from 30.5° to 34.5° 2θ for the sample **I**, where most intensive peaks of HA are expected. Tick marks below the patterns correspond to the positions of the Bragg reflections expected for the HA structure. The positions of the most intense diffraction peaks for the OCP and DCPA are shown by asterisk and plus, respectively

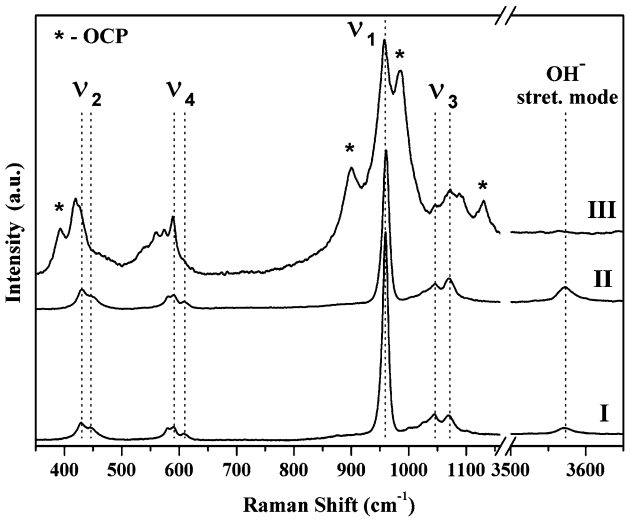

Fig. 3 Raman spectra collected from the samples **I**, **II** and **III**. Raman spectrum collected from the sample **IV** is almost identical to spectrum from sample **III**, and omitted for clarity

*Samples **I** and **II***

These Raman spectra show very strong characteristic peak at ~960 cm^{-1} due to the symmetric stretching mode $v_1(PO_4)$. Apart from this v_1 mode, two $v_2(PO_4)$ (~437 cm^{-1}), three $v_3(PO_4)$, (~1046 cm^{-1}), and four $v_4(PO_4)$ (~593 cm^{-1}) are also observed [29]. Band at 3570 cm^{-1} corresponds to stretching vibration of OH^- groups.

*Sample **III** and **IV***

Since the OCP is the phase most abundant in sample **III** according to XRD, its Raman spectrum is predominantly similar to spectra reported for this calcium phosphate [30]. OCP contains both HPO_4^{2-} and apatitic PO_4^{3-} groups in its structure. Thus, the Raman spectrum contains bands similar to those observed in samples **I** and **II** for modes v_1, v_2, v_3 and v_4, even if these bands are shifted. In addition, new peaks due to HPO_4^{2-} appear at 1130, 985, 900 and 392 cm^{-1} [30]. The disappearance of the band due to the OH^- stretching mode is explained because OCP, the principal phase in sample **III**, does not contain OH^- groups in its crystal structure. It should be emphasized that practically no differences in the intensity and band positions for the **IV** (not shown) and **III** samples were detected by Raman scattering, indicating absence of any significant change in their abundant phase composition and local structure. The observed band positions for sample **IV** are in very good agreement with published data for the OCP phase [30].

Diffuse reflectance infrared Fourier-transformed spectroscopy

The chemical and structural composition of the product was studied by IR, an useful technique to determinate the incorporation of anions, such as CO_3^{2-} and/or HPO_4^{2-}, to the crystal lattice of the as-produced powders, since XRD measurement can only clarify the average and static symmetry.

Figure 4 shows the spectra from samples **I** and **II**, which are characteristic of HA. Peaks at 3572 and 638 cm^{-1} corresponds to the stretching (v_s) and librational modes (v_L) of the hydroxyl group, respectively. Also harmonic overtones and/or combination bands appear at 2075 and 1992 cm^{-1} [29]. Bands derived from the group PO_4^{3-} appear at 1103, 1068 and 1028 cm^{-1} (attributed to the triply degenerated asymmetric stretching mode vibration—v_3); 962 cm^{-1} (symmetric stretching mode of the P–O bond—v_1); 605, 577 and 563 cm^{-1} (triply degenerated bending mode of the O–P–O bond—v_4) [29]. In addition, there are also bands that confirm the existence of carbonate ions, which indicate that the samples obtained with this hydrothermal synthesis are not stoichiometric HA, but carbonated [29]. If the CO_3^{2-} ions are occupying the OH^- sites, carbonated HA (CO_3HA) is designated as an A-type, while if they are in the PO_4^{3-} positions, CO_3HA is considered as B-type. According to the assignation of anion CO_3^{2-} [31], sample **I** and **II** can be referred as AB-type, since peaks due to type A (at 1544 and 879 cm^{-1}) and type B (at 1454, 1421 and 874 cm^{-1}) appears in the spectra.

This fact is proved well by the representative combustion bulk elemental analysis, which shows that the samples **I** and **II** contained 0.61 and 0.54 wt.% of carbon, respectively.

It should be noted that the band at 874 cm^{-1} can also be attributed to (P–OH) mode of HPO_4^{2-} group, but as can be seen in Fig. 4, the other two characteristic vibrational bands of this anion at ~980 and ~1080 cm^{-1} do not appear [32], so HA in sample **I** and **II** does not incorporate HPO_4^{2-} ions. In addition, the absence of bands at 1382 cm^{-1} indicates that NO_3^- ions coming from reactants are not included in the crystalline structure of as-produced HA [33].

Scanning electron microscopy

The morphologies of the hydrothermally produced powders, observed by SEM, are shown in Fig. 5.

Figure 5a shows a typical SEM image of the sample **I**. This sample mostly consists of the particles with plate-like morphology exhibiting a non-uniform size distribution. Also, particles with hexagonal shape have been barely observed. By contrast, SEM observations of the sample **II** (Fig. 5b) reveal a large quantity of whiskers with well-defined hexagonal morphology (one is shown in the inset to Fig. 5b) with typical widths of 0.7–3.0 μm and with lengths in the range from 3.8 μm to 9.1 μm. It should be noted that plate-like structures were almost not detected by SEM for this sample, and it can be seen that hexagonal prisms are the principal shape in sample **II**. Energy-dispersive X-ray spectroscopy (EDX) on samples **I** and **II** showed that the average molar ratios of the calcium and

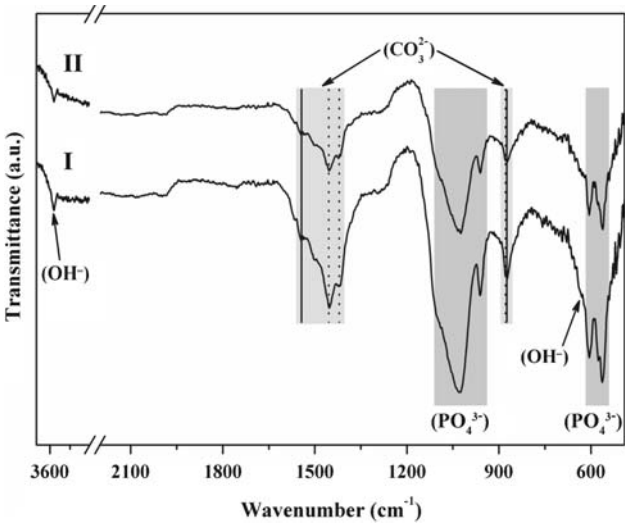

Fig. 4 IR spectra collected from the as-produced phase pure HA samples **I** and **II**. *Solid lines* are characteristic of A-type HA (partial substitution of the OH^- by CO_3^{2-}) while *dotted lines* are characteristic of B-type HA (partial substitution of the PO_4^{3-} by CO_3^{2-})

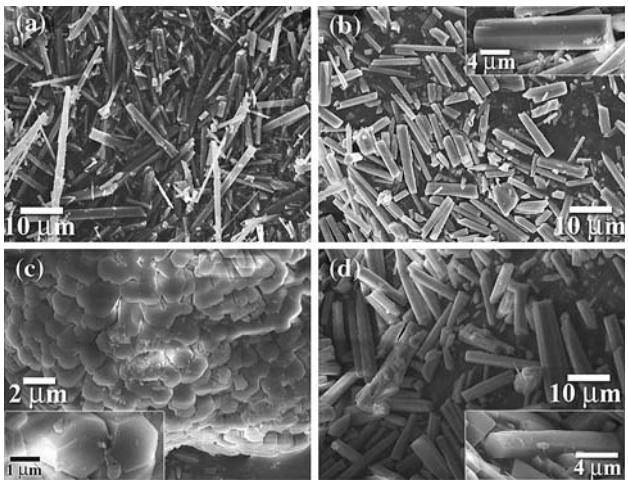

Fig. 5 SEM microphotographs are shown for hydrothermally prepared HA whiskers with the insets showing the observed well-defined hexagonal shape: (**a**) **I**, (**b**) **II**, (**c**) **III** and (**d**) **IV**

phosphorous elements (Ca/P) are ~1.76 for sample **I** and ~1.74 for sample **II**; these values are in good agreement with the stoichiometric value for HA (Ca/P = 1.67) as well as with the initial molar ratio under hydrothermal synthesis.

SEM observations of sample **III** (Fig. 5c) shows the presence of two types of well crystallized structures in the sample—mainly plate-like shapes, attributed to the OCP abundant phase [34], and big aggregates consisting of sharp faceted hexagonal crystals with quite uniform widths of about ~1.5 μm (inset in Fig. 5c). These big agglomerates of hexagons were determined to be hydroxyapatite by EDX analysis. The average molar ratio of the calcium and phosphorous elements (Ca/P) is ~1.73, which is more close to the stoichiometric value for HA (Ca/P = 1.67) than those for OCP (Ca/P = 1.33) and/or DCPA (Ca/P = 1.00). The general morphology of the sample **IV** is quite similar to that of sample **III**, with mainly plate-like structures corresponding to the OCP phase, but at the same time, the presence of non-agglomerated whiskers was also observed. The typical SEM image of a whisker region is shown in Fig. 5d. It should be emphasized, that these whiskers possess a sharp faceted hexagonal morphology (see inset to Fig. 5d) with relatively uniform size distribution with an average width of ~2.5 μm and an average length of ~14 μm, as was established from a detailed particle size analysis of 50 whiskers from several SEM micrographs. The EDX analysis of sample **IV** shows that overall Ca/P ratio in the whisker regions is ~1.72, indicating that those whiskers are HA. It should be note that the values of Ca/P ratio in hydrothermal synthesis products are higher than that of stoichiometric HA, which is believed to result from a partial substitution of the phosphate and hydroxide groups in the HA lattice by carbonate ions, in agreement with IR and elemental analyses.

Transmission electron microscopy

Transmission electron microscopy was applied to investigate the microstructure of the whiskers and the observed results are in agreement with SEM and XRD data. Figure 6a shows a typical low-magnification TEM image of as-prepared whiskers of sample **II**. The sample mostly consists of well defined and sharp faceted rod-like crystals with mean diameters of 0.7–1.0 μm, in good agreement with the SEM data. The inset in Fig. 6a is a typical electron diffraction pattern corresponding to the terminal end of HA whisker. ED reveals a high crystallinity of the whiskers, which was also confirmed by XRD. The dots of the ED pattern can be completely indexed in the HA hexagonal $P6_3/m$ space group, using the HA unit cell parameters of JCPDS No. 72-1243. It should be noted that all electron diffraction patterns along the long-axis of the whisker have the same geometry, which was subsequently confirmed to be a common feature of almost all whiskers in sample **II**, thus revealing that each HA whisker is a single crystal. The terminal end of HA whisker in Fig. 6a is shown on Fig. 6b, which reveals the presence of a local deformation in the synthesized whiskers. HRTEM analysis (Fig. 6c) of an edge area of the terminal end of HA whisker also indicates that the whisker is highly crystalline. The crystal lattice can be estimated to be about 8.2 and 3.4 Å, corresponding to the (210) and (002) planes of the hexagonal crystal structure of HA, respectively, indicating that the hydroxyapatite whisker grow along the *c*-axis, which is in good agreement with XRD data, discussed above.

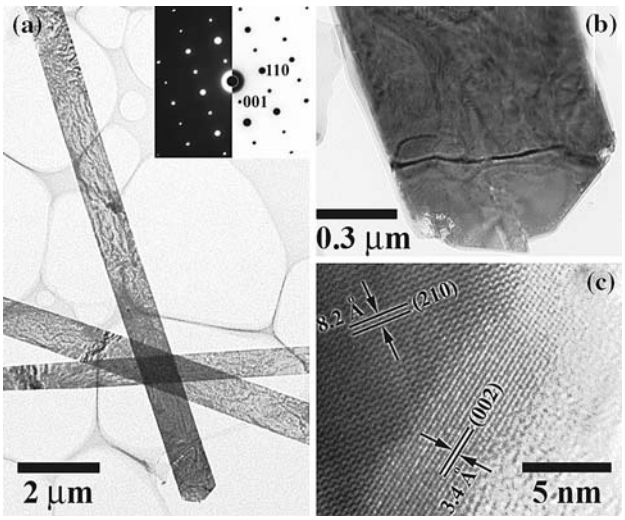

Fig. 6 (**a**) A low-magnification TEM image and corresponding ED pattern (inset) of HA whiskers of sample **II**; (**b**) TEM image of the terminal end of HA whisker in (**a**); (**c**) HRTEM image of an edge area of the lamellar terminal end of HA whisker in (**b**), with (210) and (002) lattice planes visible

Discussion

In our investigation, samples **I** and **II** are the products of the hydrothermal reaction between $Ca(NO_3) \cdot 4H_2O$ and $(NH_4)_2HPO_4$ at 90 °C for 72 h and Scheme 1 temperature cycle (Fig. 1), respectively, in presence of urea. According to XRD, powders **I** and **II** are pure HA hexagonal phases which is also confirmed by Raman spectroscopy. Moreover, powder XRD results demonstrate that the particles in as-prepared samples **I** and **II** are mainly oriented along the *c*-axis direction of the hexagonal crystal structure [28]. SEM investigation clearly indicates the presence of whisker structures with well-defined hexagonal prism morphology, especially in case of sample **II**. TEM/ED/HRTEM confirms that the whiskers in the sample **II** are single crystals, sharp faceted and oriented with their axis along *c*-axis. Existence of local deformations in hydrothermally prepared whiskers was also revealed by TEM.

It is to be noted that IR spectroscopy provides important information about the local and dynamic state of whiskers. For samples **I** and **II** it reveals that they are not stoichiometric HA owing to a partial substitution of the both PO_4^{3-} and OH^- groups by carbonate anion, indicating CO_3HA formation (type AB). Biological HA has multiple substitutions and deficiencies at all ionic sites and contains 3–5 wt.% carbonate groups [35], thus obtaining CO_3HA whiskers is the requirement rather than a problem for its application for a biodegradable bioceramics [36]. Apparently, carbonate anions come from the urea decomposition into $NH_{3(aq)}$ and $CO_{2(g)}$. Although $CO_{2(g)}$ is mostly released from the system through the porous PTEF gasket, however it's also partially dissolved into the water, and therefore, easily incorporated into HA product due its strong ability to incorporate different ions [35].

It was established that the optimal initial pH values resulting in the pure HA phase formation lay in the range of 3.0–3.5. For the sample **I** the initial pH was 3.0 while after hydrothermal reaction it becomes 8.4 due to the urea decomposition, and thus providing the proper condition for the phase pure HA formation, according to the solubility diagrams of calcium phosphates [37]. HA cannot be synthesized directly at the initial pH and the synthesis must proceed through multiple steps; first the formation of DCPA, following the formation of OCP, which should act as the precursors for the final HA whiskers formation [35].

SEM observation shows that in sample **I**, HA mainly retains the plate-like morphology of OCP [34], which is because of the similarities between its structures, and OCP act as a template for epitaxial growth of HA [38]. In order to increase the quantity of hexagonal whiskers, a gradual increase of the pH in the reaction medium (sample **II**) was

performed by varying the temperature between 70 °C and 90 °C, followed by ramping at 90 °C for 12 h in the range of urea decomposition (Fig. 1, Scheme 1). Such gradual increasing ensures a low speed of HA nucleus formation as well as slow crystallization of hexagonal whiskers of HA, thus excluding the intensive epitaxial growth from the OCP template. SEM images of sample **II** reveal that the quantity of particles with hexagonal well-defined prism morphology is highest in present study and considerably larger in comparison with sample **I**, but at the same time, the size distribution of the as-produced whiskers is non-uniform.

In light of this, one very important question appears, can we control the HA whisker size distribution in the products? In order to verify this question, the synthesis with another temperature cycle of hydrothermal treatment (Fig. 1, Scheme 2) which is similar to the mentioned above including one addition ramp step at 70 °C for 1 h was performed (Table 1, samples **III** and **IV**) with respect to more gradual increasing of the pH.

According to XRD and Raman spectroscopy, syntheses by Scheme 2 resulted in the reduction of yield of the title compound. For example, in case of sample **III** OCP is a most abundant phase, consequently, large quantity of plate-like structures, attributed to the OCP morphology [34], were detected by SEM in this powder. Taking into account that the final pH of the reaction solution for sample **III** was 6.9, it is believed that 72 h is not enough for the proper degree of urea decomposition under this cycle and therefore leads to the low yield of HA phase under Scheme 2 process (Fig. 1). According to XRD, content of HA in sample **III** is ~30 wt.%. SEM reveals that HA structures are mostly gathered in big aggregates with a radial growth consisting of hexagonal crystals with quite uniform widths of about ~1.5 μm.

To avoid such aggregation, an additional synthesis with CTAB as a surfactant was carried out (sample **IV**). In addition, the cation surfactant CTAB ionizes completely in an aqueous system, resulting in an amino cation with tetrahedral structure. Owing to the charge and structure complementarity, these positive headgroups may bond to the phosphate reactant, PO_4^{3-} ions, which are also tetrahedral in structure, and thus provide a control of the crystallization process [39]. As a result, the growth of HA with rod-like morphology is expected to be a favor at low pH [40]. SEM images show that the HA whiskers formed in this case possess relatively uniform size distribution. This results from samples **III** and **IV** suggest that the slow control of the pH increase by controlling the urea decomposition, provide the conditions for the HA crystallization to form more uniform structures. At the same time, the low value of final pH obtained for these samples and its phase composition, also show that not all the urea is decomposed, establishing the fact that pH has not increased enough to continue the hydrolysis of precursors to form HA.

The achievement of a uniform distribution and controlled growth of whiskers based on HA has great importance in improving the mechanical properties of hydroxyapatite ceramics. The mechanism of the whiskers crystallization and growth under hydrothermal conditions is therefore under investigation.

Conclusions

Hydroxyapatite whiskers were successfully produced by a simple approach, based on the reaction between $Ca(NO_3) \cdot 4H_2O$, $(NH_4)_2HPO_4$ and urea under hydrothermal conditions. Investigation of the influence of the temperature and duration of the hydrothermal treatment as well as the initial pH value on the phase composition of the product has resulted in the optimization of the synthetic conditions, leading to the large quantity synthesis. Gradual increase of the pH technique and the use of surfactant during the synthesis allowed producing single-crystalline whiskers with sharp faceted hexagonal prism morphology elongated along the *c*-axis of the apatite crystal structure.

Acknowledgements We are grateful to Dr. Yu. V. Kolen'ko and Prof. M. Aizawa for the fruitful discussion. The work is partially supported by the Spanish Ministry of Science and Technology, under the project MAT2002-03857.

References

1. Suchanek W, Yoshimura M (1998) J Mater Res 13:94
2. Barralet JE, Grover L, Gaunt T, Wright AJ, Gibson IR (2002) Biomaterials 23:3063
3. Hench LL (1991) J Am Ceram Soc 74:1487
4. Dorozhkin SV, Epple M (2002) Angew Chem Int Ed Engl 41:3130
5. Ong JL, Chan DC (2000) Crit Rev Biomed Eng 28:667
6. Bohner M (2001) Key Eng Mater 192–195:765
7. Park K, Sundaresan S, Vasilos T, Sung C (1994) J Mater Res 9:2476
8. Ruys AJ, Wei M, Milthorpe BK, Brandwood A, Sorrell CC (1993) J Aust Ceram Soc 29:51
9. De With G, Corbijn AJ (1989) J Mater Sci 24:3411. doi: 10.1007/BF01139073
10. Ioku K (1998) In: Amjad Z (ed) Calcium phosphates in biological and industrial systems. Kluwer, Boston, p 357
11. Yubao L, De Groot K, De Wijn J, Klein CPAT, Meer SVD (1994) J Mater Sci Mater Med 5:326
12. Yoshimura M, Suda H, Okamoto K, Ioku K (1994) J Mater Sci 29:3399. doi:10.1007/BF00352039
13. Suchanek W, Yashima M, Kakihana M, Yoshimura M (1997) J Am Ceram Soc 80:2805
14. Fujishiro Y, Yabuki H, Kawamura K, Sato T, Okuwaki A (1993) J Chem Tech Biotechnol 57:349
15. Zhang H, Yan Y, Wang Y, Li S (2002) Adv Eng Mater 4:916

16. Kandori K, Horigami N, Yasukawa A, Ishikawa T (1997) J Am Ceram Soc 80:1157
17. Mizutani Y, Hattori M, Okuyama M, Kasuga T, Nogami M (2005) J Eur Ceram Soc 25:3181
18. Taş AC (2001) J Am Ceram Soc 84:295
19. Lu X, Zhao Z, Leng Y (2005) J Cryst Growth 284:506
20. Wang X, Zhuang J, Peng Q, Li Y (2006) Adv Mater 18:2031
21. Liu J, Ye X, Wang H, Zhu M, Wang B, Yan H (2003) Ceram Int 29:629
22. Fujishiro Y, Yabuki H, Kawamura K, Sato T, Okuwaki A (1993) J Chem Tech Biotechnol 57:349
23. Park HC, Baek DJ, Park YM, Yoon SY, Stevens R (2004) J Mater Sci 39:2531. doi:10.1023/B:JMSC.000002021.82216.6b
24. Aizawa M, Kinoshita M, Yamada K, Itatani K, Kishioka A (1998) Inorg Mater 5:387
25. Ioku K, Yamauchi S, Fujimori H, Goto S, Yoshimura M (2002) Solid State Ionics 151:147
26. Andrés-Vergés M, Fernández-González C, Martínez-Gallego M (1998) J Eur Ceram Soc 18:1245
27. Yao J, Tjandra W, Chen YZ, Tam KC, Ma J, Soh B (2003) J Mater Chem 13:3053
28. Aizawa M, Ueno H, Itatani K, Okada I (2006) J Eur Ceram Soc 26:501
29. Koutsopoulos S (2002) J Biomed Mater Res 62:600
30. Sauer GR, Zunic WB, Durig JR, Wuthier RE (1994) Calcif Tissue Int 54:414
31. Monma H, Takahashi T (1987) Gypsum lime 210:287
32. Steger E, Herzog K (1964) Anorg All Chem 331:169
33. Nakamoto K (1997) Infrared and Raman spectra of inorganic and coordination compounds, part B: applications in coordination, organometallic and bioinorganic chemistry, 5th edn. Wiley, New York, p 87
34. Brown WE (1962) Nature 196:1048
35. Elliot JC (1994) Structure and chemistry of the apatites and other calcium ortophosphates. Elsevier, Amsterdam, p 80, 154, 260
36. Ison IC, Fulmer MT, Barr BM, Constanz BR (1994) In: Brown PW, Constanz B (eds) Hydroxyapatite and related materials. CRC Press, Boca Raton FL, p 215
37. Levin EM, Robbins CR and Mcmurdie HF (1964) Phase diagrams for ceramist, vol I. American Ceramic Society, Columbus, OH, fig. 246
38. Brown WE, Smith JP, Lehr JR, Frazier AW (1962) Nature 196:1050
39. Li Y, Li YD, Deng ZX (2001) Int J Inorg Mater 3:633
40. Wang YJ, Chen JD, Wei K, Zhang SH, Wang XD (2006) Mater Lett 60:3227